A&A 448, 439–446 (2006)
DOI: 10.1051/0004-6361:20053526

Astronomy & Astrophysics

The excursion set approach, and an improved model for the multiplicity function⋆

A. Del Popolo[1,2,3]

[1] Dipartimento di Matematica, Università Statale di Bergamo, via dei Caniana 2, 24127 Bergamo, Italy
[2] Boğaziçi University, Physics Department, 80815 Bebek, Istanbul, Turkey
e-mail: antonino.delpopolo@boun.edu.tr
[3] Istanbul Technical University, Ayazaga Campus, Faculty of Science and Letters, 34469 Maslak/Istanbul, Turkey

Received 27 May 2005 / Accepted 18 October 2005

ABSTRACT

I compare numerical multiplicity function with the theoretical multiplicity function obtained by means of the excursion set model and an improved version of the barrier shape which implicitly takes account of total angular momentum acquired by the proto-structure during evolution and of a non-zero cosmological constant. I describe the better agreement of the multiplicity function obtained in this paper with simulations of other previous models. While the theoretical multiplicity function of the present paper is in agreement with high resolution N-body simulations, the comparison of the theoretical multiplicity function of the present paper with the theoretical multiplicity function of several authors shows some discrepancies: e.g., the maximum value of the multiplicity function from simulations at $\nu \sim 1$ is smaller, and its low mass tail is shallower when compared with the ST multiplicity function.
The multiplicity function of the present paper gives a good fit to simulations results and was obtained from a sound theoretical background.

Key words. cosmology: theory – large-scale structure of Universe – galaxies: formation

1. Introduction

It is likely that structures in the Universe grow from small initially Gaussian density perturbations that progressively detach from the general expansion, reach a maximum radius and then collapse to form bound objects. Larger haloes are formed hierarchically by mergers between smaller ones.

Two different kinds of method are widely used for the study of structure formation. The first one is N-body simulations that are able to follow the evolution of a large number of particles under the influence of the mutual gravity, from initial conditions to the present epoch. The second one is semi-analytical methods. Among them, the Press-Schechter (hereafter PS) approach and its extensions (EPS) are of great interest since they allow us to compute mass functions (Press & Schechter 1974; Bond et al. 1991), to approximate merging histories (Lacey & Cole 1993, LC93 hereafter; Bower 1991; Sheth & Lemson 1999b) and to estimate the spatial clustering of dark matter haloes (Mo & White 1996; Catelan et al. 1998; Sheth & Lemson 1999a).

In the PS and Bond et al. (1991) papers, the authors described how the statistical properties of the initial density field, assumed to be Gaussian, together with the spherical collapse model, could be used to derive an estimate of the number density of collapsed dark matter haloes at later times: the so-called universal "unconditional" multiplicity function. Lacey & Cole (1993) showed how the model could be extended to estimate the merging rate of small objects to form larger ones, thus leading to the possibility of estimating the "conditional" mass function of sub-haloes within parent haloes. Mo & White (1996) applied the model to compute an approximation of the spatial clustering of dark haloes.

Although the analytical framework of the PS model has been greatly refined and extended, it is well known that the PS mass function, while qualitatively correct, disagrees with the results of N-body simulations. In particular, the PS formula overestimates the abundance of haloes near the characteristic mass M_* and underestimates the abundance in the high mass tail (Efstathiou et al. 1988; Lacey & Cole 1994; Tozzi & Governato 1998; Gross et al. 1998; Governato et al. 1999).

A better agreement between the numerical mass function and the analytic mass function can be obtained by incorporating into the PS ansatz the non-sphericity of collapse model (Del Popolo & Gambera 1998; Sheth & Tormen 1999, hereafter ST; Sheth et al. 2001, hereafter SMT; Sheth & Tormen 2002, hereafter ST1; Jenkins et al. 2001, hereafter J01), instead of the spherical model or taking into account the spatial correlation of density fluctuations (Nagashima 2001).

However, different authors support different mass functions. More recently in order to investigate the functional form

⋆ Appendices A and B are only available in electronic form at http://www.edpsciences.org

of the universal multiplicity function, Yahagi et al. (2004) (hereafter YNY) performed five runs of N-body simulations with high mass resolution and compared them with different multiplicity function and with a fit proposed by them.

They showed that discrepancies are observed between some of the quoted analytical multiplicity function and simulations: for example the maximum value of the multiplicity function from their simulations at $\nu \simeq 1$ is smaller, and its low mass tail is shallower when compared to the ST multiplicity function.

In the present paper, I use an improved version of the barrier shape obtained in Del Popolo & Gambera (1998), obtained from the parameterization of the nonlinear collapse discussed in that paper, taking account of asphericity and tidal interaction between protohaloes and the effects of a non-zero cosmological constant, together with the results of ST1 in order to study the "unconditional" mass function.

As previously reported, multiplicity functions like ST and J01 fit high resolution N-body simulations like those of YNY only approximatively, while the functional form proposed in YNY provides a better fit than the ST functional form. Unfortunately the functional form for the multiplicity function proposed in YNY and similarly that of J01 (which is a fit to their "Hubble Volume" simulations of τCDM and ΛCDM cosmologies) are not based on any theoretical background. Thus it is important to find a better analytical form which, starting from "first principles", is able to fit simulations better and is physically motivated. I show that the function obtained in this paper, similarly to that in YNY, provides a better fit than the ST or other functional forms used in the literature and moreover it has been obtained from solid physical, theoretical, arguments.

As previously reported, a comparison between ST multiplicity functions with the YNY simulations and with the result of the present paper shows a slight difference which is larger at small ν. The difference between the mass functions reflects the difference between the barrier obtained by ST and that used in this paper.

The present paper is based on a more sophisticated calculation of the barrier based on an improved collapse model that takes into account angular momentum acquisition by proto-structures (see Del Popolo & Gambera 1998) and the effects of a non-zero cosmological constant.

The paper is organized as follows: in Sect. 2, I calculate the "unconditional" multiplicity function. Section 3 is devoted to a discussion of the N-body simulations used for the comparison with the theoretical multiplicity function of the present paper, Sects. 4 and 5 are devoted to results and to conclusions, respectively.

2. The barrier model and the multiplicity function

The PS model when compared to numerical simulations gives a smaller number of high-mass halos while giving a larger number of low-mass halos. The quoted discrepancy that leads to research on new expressions for the mass function is not surprising since the PS model, as any other analytical model, should make several assumptions to obtain simple analytical predictions. The main assumptions that the PS model combines are the simple physics of the spherical collapse model with the assumption that the initial fluctuations were Gaussian and small. On average, initially denser regions collapse before less dense ones, which means that, at any given epoch, there is a critical density, $\delta_c(z)$, which must be exceeded if collapse is to occur. In the spherical collapse model, this critical density does not depend on the mass of the collapsed object. Taking account of the effects of asphericity and tidal interaction with neighbors, it is possible to show that it is mass dependent (Del Popolo & Gambera 1998, SMT). Also, the Gaussian nature of the fluctuation field means that a good approximation to the number density of bound objects that have mass m at time z is given by considering the barrier crossing statistics of many independent and uncorrelated random walks, where the barrier shape $B(m, z)$, is connected to the collapse threshold. Simply changing the barrier shape, SMT showed that it is possible to incorporate the "quoted effects"[1] in the excursion set approach. Moreover, using the shape of the modified barrier in the excursion set approach, it is possible to obtain a good fit to the universal halo mass function[2]. The excursion set approach allows one to calculate good approximations to several important quantities, such as the "unconditional" and "conditional" mass functions. ST1 provided formula to calculate these last quantities starting from the shape of the barrier.

In the following, I use an improved version of the barrier obtained in Del Popolo & Gambera (1998) to get the multiplicity functions to compare to those obtained by PS, ST, J01, YNY and with numerical simulations of YNY. Since the way the barrier is obtained is described in previous papers (see Del Popolo & Gambera 1998, 1999, 2000) the reader is referred to those papers for details. Assuming that the barrier is proportional to the threshold for the collapse, similarly to ST, the barrier can be expressed, in the case of a zero cosmological constant, in the form:

$$B(M) = \delta_c = \delta_{co}\left[1 + \int_{r_i}^{r_{ta}} \frac{r_{ta} L^2 \cdot dr}{GM^3 r^3}\right] \simeq \delta_{co}\left[1 + \frac{\beta_1}{\nu^{\alpha_1}}\right] \quad (1)$$

where $\delta_{co} = 1.68$ is the critical threshold for a spherical model, r_i is the initial radius, r_{ta} is the turn-around radius, L the angular momentum, $\alpha_1 = 0.585$ and $\beta_1 = 0.46$. The angular momentum appearing in Eq. (1) is the total angular momentum acquired by the proto-structure during evolution. In order to calculate L, I use the same model as described in Del Popolo & Gambera (1998, 1999) (more hints on the model and some of the model limits can be found in Del Popolo et al. (2001) and in Appendix A to the present paper).

Assuming a non-zero cosmological constant Eq. (1) is changed as follows (see Appendix B):

$$\begin{aligned} B(M) &= \delta_c = \delta_{co}\left[1 + \int_{r_i}^{r_{ta}} \frac{r_{ta} L^2 \cdot dr}{GM^3 r^3} + \Lambda \frac{r_{ta} r^2}{6GM}\right] \\ &\simeq \delta_{co}\left[1 + \frac{\beta_1}{\nu^{\alpha_1}} + \frac{\Omega_\Lambda \beta_2}{\nu^{\alpha_2}}\right] \end{aligned} \quad (2)$$

[1] In the case of objects collapsing at the same time, the less massive regions must initially have been denser than the more massive ones.

[2] Note that at present there is no good numerical test of analytic predictions for the low mass tail of the mass function.

where $\alpha_2 = 0.4$ and $\beta_2 = 0.02$ and Ω_Λ is the contribution to the density parameter from the cosmological constant.

The CDM spectrum used in this paper is that of Bardeen et al. (1986, hereafter BBKS, Eq. (G3)), with the transfer function:

$$T(k) = \frac{[\ln(1+2.34q)]}{2.34q} \times \left[1 + 3.89q + (16.1q)^2 + (5.46q)^3 + (6.71)^4\right]^{-1/4} \quad (3)$$

where $q = \frac{k\theta^{1/2}}{\Omega_\chi h^2 \mathrm{Mpc}^{-1}}$. Here $\theta = \rho_{\rm er}/(1.68\rho_\gamma)$ represents the ratio of the energy density in relativistic particles to that in photons ($\theta = 1$ corresponds to photons and three flavors of relativistic neutrinos). The power spectrum was normalized to reproduce the observed abundance of rich clusters of galaxies (e.g. Bahcal & Fan 1998).

It is important at this point to present a clear definition of the "multiplicity function" and its correlation with the usual, more straightforwardly used, "mass function".

Following Sheth & Tormen (1999) notation, if $f(m,\delta)\mathrm{d}m$ denotes the fraction of mass that is contained in collapsed haloes that have masses in the range m–$m + \mathrm{d}m$, at redshift z, and $\delta(z)$ the redshift dependent overdensity, the associated "unconditional" mass function is:

$$n(m,\delta)\mathrm{d}m = \frac{\overline{\rho}}{m} f(m,\delta)\mathrm{d}m. \quad (4)$$

In the excursion set approach, the universal or "unconditional" mass function, $n(m,z)$, representing the average comoving number density of haloes of mass m is given by:

$$n(m,z) = \frac{\overline{\rho}}{m^2}\frac{\mathrm{d}\log\nu}{\mathrm{d}\log m}\nu f(\nu) \quad (5)$$

(Bond et al. 1991), where $\overline{\rho}$ is the background density, $\nu = \left(\frac{\delta_{\rm c}(z)}{\sigma(m)}\right)^2$ is the ratio between the critical overdensity required for collapse in the spherical model, $\delta_{\rm c}(z)$, to the rms density fluctuation $\sigma(m)$, on the scale r of the initial size of the object m. The function $\nu f(\nu)$ is the "multiplicity function" which is obtained by computing the distribution of first crossings, $f(\nu)\mathrm{d}\nu$, of a barrier $B(\nu)$, by independent, uncorrelated Brownian motion random walks. The multiplicity function and mass function are related by Eq. (5). In the literature sometime the terms "mass function" and "multiplicity function" are used as synonymous (e.g. ST; Lin et al. 2002).

The mass function thus can be calculated once a shape for the barrier is given and the power spectrum is known. In the case of spherical collapse, characterized by a constant barrier (for all ν), PS and Bond et al. (1991) obtained:

$$\nu f(\nu) = \left(\frac{2}{\pi}\right)^{\frac{1}{2}} \sqrt{\nu}\exp\left(-\frac{\nu}{2}\right). \quad (6)$$

In the case of a nonspherical collapse, the shape of the barrier is no longer a constant and moreover it depends on mass (Del Popolo & Gambera 1998; SMT). As shown by ST1, for a given barrier shape, $B(S)$, where $S \equiv S_*\left(\frac{\sigma}{\sigma_*}\right)^2 = \frac{S_*}{\nu}$ and $\sigma_* = \sqrt{S_*} = \delta_{\rm co}$, the first crossing distribution is well approximated by:

$$f(S)\mathrm{d}S = |T(S)|\exp\left(-\frac{B(S)^2}{2S}\right)\frac{\mathrm{d}S/S}{\sqrt{2\pi S}} \quad (7)$$

where $T(S)$ is the sum of the first few terms in the Taylor expansion of $B(S)$:

$$T(S) = \sum_{n=0}^{5}\frac{(-S)^n}{n!}\frac{\partial^n B(S)}{\partial S^n}. \quad (8)$$

The quantity $Sf(S,t)$ is a function of the variable ν alone. Since $\delta_{\rm c}$ and σ evolve with time in the same way, the quantity $Sf(S,t)$ is independent of time. Setting $Sf(S,t) = \nu f(\nu)$, one obtains the so-called function $f(\nu)$. This is why the shape of the barrier influences the form of the multiplicity function.

The previous Eqs. (7) and (8), reduce to Eq. (6) for constant barriers. In the case of the ellipsoidal barrier shape given in ST:

$$B\left(\sigma^2, z\right) = \sqrt{a}\delta_{\rm c}(z)\left[1 + \frac{\beta}{(a\nu)^\alpha}\right]. \quad (9)$$

Equations (7) and (8), give, after truncating the expansion at $n = 5$ (see ST):

$$\nu f(\nu) = \sqrt{a\nu/2\pi}\left[1 + \beta(a\nu)^{-\alpha}g(\alpha)\right] \times \exp\left(-0.5a\nu\left[1 + \beta(a\nu)^{-\alpha}\right]^2\right) \quad (10)$$

where

$$g(\alpha) = \left|1 - \alpha + \frac{\alpha(\alpha-1)}{2!} - \ldots - \frac{\alpha(\alpha-1)\cdots(\alpha-4)}{5!}\right|. \quad (11)$$

If the barrier takes account of the cosmological constant, as in Eq. (2), using the same method that lead to Eq. (10), we have that:

$$\nu f(\nu) = A_1\left(1 + \frac{\beta_1 g(\alpha_1)}{(a\nu)^{\alpha_1}} + \frac{\beta_2 g(\alpha_2)}{(a\nu)^{\alpha_2}}\right)\sqrt{\frac{a\nu}{2\pi}} \times \exp\left\{-a\nu\left[1 + \frac{\beta_1}{(a\nu)^{\alpha_1}} + \frac{\beta_2}{(a\nu)^{\alpha_2}}\right]^2/2\right\}. \quad (12)$$

Using the values for β and α of ST ($a = 0.707$, $\delta_{\rm c}(z) = 1.686(1+z)$, $\beta \simeq 0.485$ and $\alpha \simeq 0.615$) in Eq. (10), one gets (ST1):

$$\nu f(\nu) \simeq A_2\left(1 + \frac{0.094}{(a\nu)^{0.6}}\right)\sqrt{\frac{a\nu}{2\pi}} \times \exp\left\{-a\nu\left[1 + \frac{0.5}{(a\nu)^{0.6}}\right]^2/2\right\} \quad (13)$$

with $A_2 \simeq 1$. This last result is in good agreement with the fit of the simulated first crossing distribution (ST):

$$\nu f(\nu)\mathrm{d}\nu = A_3\left(1 + \frac{1}{(a\nu)^p}\right)\sqrt{\frac{a\nu}{2\pi}}\exp(-a\nu/2) \quad (14)$$

where $p = 0.3$, and $a = 0.707$.

The normalizatition factor A_3 has to satisfy the constraint:

$$\int_0^\infty f(\nu)\mathrm{d}\nu = 1 \quad (15)$$

and as a consequence it is not an independent parameter, but is expressed in the form:

$$A_3 = \left[1 + 2^{-p}\pi^{-1/2}\Gamma(1/2 - p)\right]^{-1} = 0.3222\,^3. \quad (16)$$

In the case of the barrier given in Eq. (1), the "unconditional" multiplicity function can be approximated by:

$$\nu f(\nu) \simeq A_4\left(1 + \frac{b}{(a\nu)^{0.585}}\right)\sqrt{\frac{a\nu}{2\pi}} \times \exp\left\{-ac\nu\left[1 + \frac{d}{(a\nu)^{0.585}}\right]^2\right\} \quad (17)$$

where $a = 0.707$, $b = 0.1218$, $c = 0.4019$, $d = 0.5526$ and $A_4 \simeq 1.75$ is obtained from the normalization condition.

In the case of the barrier with non-zero cosmological constant, Eq. (2), a good approximation to the multiplicity function is given by:

$$\nu f(\nu) \simeq A_5\left(1 + \frac{0.1218}{(a\nu)^{0.585}} + \frac{0.0079}{(a\nu)^{0.4}}\right)\sqrt{\frac{a\nu}{2\pi}} \times \exp\left\{-0.4019a\nu\left[1 + \frac{0.5526}{(a\nu)^{0.585}} + \frac{0.02}{(a\nu)^{0.4}}\right]^2\right\} \quad (18)$$

where $A_5 = 1.75$.

As previously reported, for matter of completeness, to the previous functions, namely PS, ST, Eq. (17) we have to add J01, which satisfies the equation:

$$\nu f(\nu) = 0.315\,\exp\left(-\left|0.61 + \ln\left[\sigma^{-1}(M)\right]\right|^{3.8}\right) = 0.315\,\exp\left(-\left|0.61 + \ln\,\sqrt{\nu} - \ln\,\delta_c\right|^{3.8}\right). \quad (19)$$

The above formula is valid for $-1.2 < \ln\,\sqrt{\nu} - \ln\,\delta_c < 1.05$. YNY (Eq. (7), hereafter YNY7) proposed the following function to fit the numerical multiplicity function:

$$\nu f(\nu) = A_6\left[1 + \left(B\,\sqrt{\nu}/\,\sqrt{2}\right)^C\right]\sqrt{\nu}^D \exp\left[-\left(B\,\sqrt{\nu}/\,\sqrt{2}\right)^2\right], \quad (20)$$

where A_6 is a normalization factor to satisfy the unity constraint, $\int_0^\infty f(\nu)\mathrm{d}\nu = 1$, therefore

$$A_6 = 2\left(B/\,\sqrt{2}\right)^D \left\{\Gamma[D/2] + \Gamma\left[(C + D)/2\right]\right\}^{-1}. \quad (21)$$

The best-fit parameters are given as $B = 0.893$, $C = 1.39$, and $D = 0.408$, and from these parameters, A is constrained so that $A_6 = 0.298$.

This best-fit function from Eq. (20) is shown in Figs. 1–3 and is only valid at $0.3 \leq \nu \leq 3$.

[3] Note, that Eq. (14) gives a better fit to Eq. (10) if $A \simeq 0.3$ and $a \simeq 0.79$. Vice versa a smaller value of a ($a \simeq 0.63$) and $A = 1.08$ in Eq. (10) gives a better fit to Eq. (14) (with $A_1 = 0.3222$ and $a = 0.707$), which was the one ST used to compare model and data.

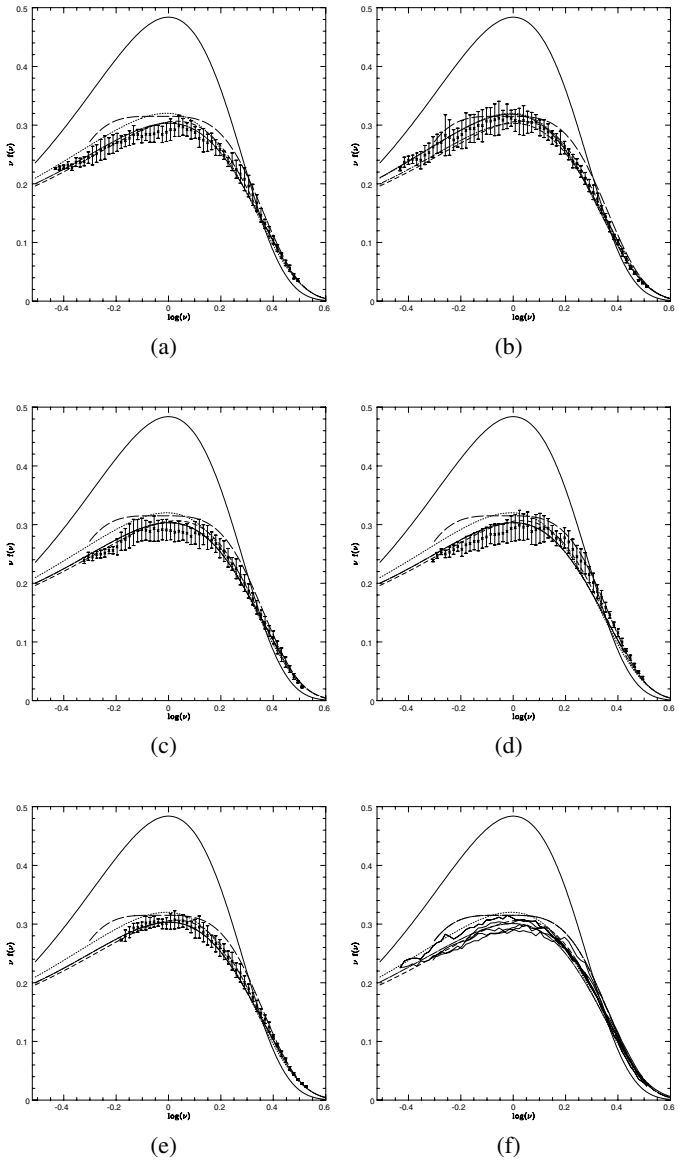

Fig. 1. Panels **a)**–**e)** plot the multiplicity functions from five runs of YNY simulations (crosses with error bars). The panel **f)** shows the results from all the runs (thin lines). In each panel, the solid line represents PS multiplicity function, the dotted line the ST multiplicity function, the long-dashed line the J01 multiplicity function, the short-dashed line YNY7, and the dot-dashed line the one of the present paper.

3. *N*-body simulations used for the comparison

The theoretical model of the present paper is compared with YNY simulations. I use the YNY simulations because the mass dynamic range is large and the mass resolution of the YNY results is high compared with other papers that try to obtain the mass function of dark halos and moreover it gives a fitting function for numerical multiplicity functions.

YNY used the Adaptive Mesh Refinement N-body code developed by Yahagi (2002), which is a vectorized and parallelized version of the code described in Yahagi & Yoshii (2001). Those simulations adopt the ΛCDM cosmological parameters of $\Omega_m = 0.3$, $\Omega_\lambda = 0.7$, $h = 0.7$, and $\sigma_8 = 1.0$, using

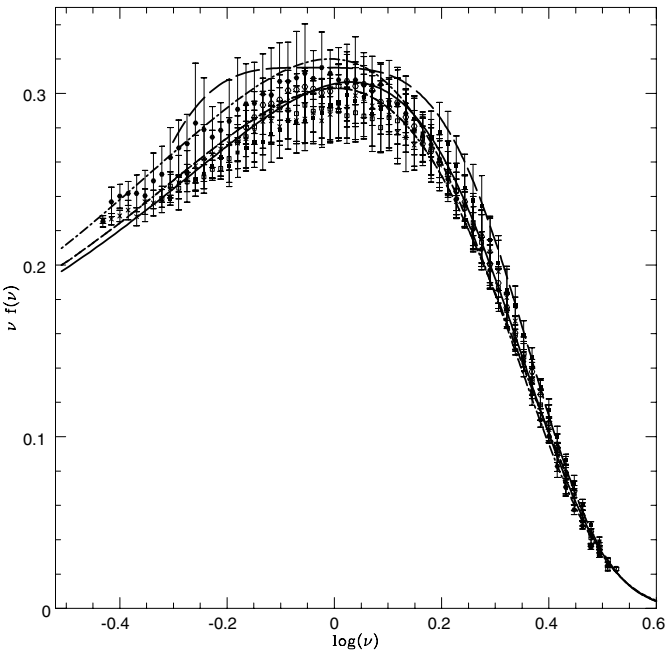

Fig. 2. The best-fit multiplicity function. In the plot the solid line represents the multiplicity function obtained in this paper, the short-dashed line YNY7, the dotted line the ST multiplicity function, the long-dashed line the J01 multiplicity function. The errorbars with open circles represent the run 140 of YNY, those with filled squares the case 70b, those with open squares the case 70a, those with filled circles the case 35b, those with crosses the case 35a.

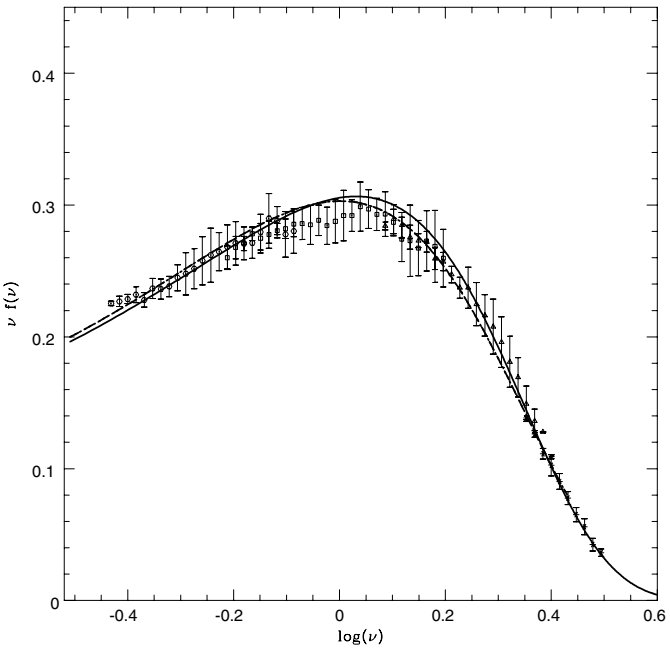

Fig. 3. Time dependence of the multiplicity function from the 35a run, for four redshift ranges of $0 \leq z < 1$ (open circles), $1 \leq z < 3$ (open squares), $3 \leq z < 6$ (open triangles), and $z \geq 6$, (crosses). Also shown are YNY7 (solid line) and the model of this paper (dot-dashed line).

512^3 particles in common. The size of the finest mesh is 1/64 of the base mesh, and the force dynamic range is $2^{15} = 32\,768$. Other simulation parameters such as the box size and the particle mass are given in Table 1 of YNY. For example, the run 35a has a box size $L = 35\ h^{-1}$ Mpc, a particle mass of $2.67 \times 10^7\ h^{-1}\ M_\odot$, and the initial redshift $z_{\rm start} = 50$. Initial conditions were generated by the GRAFIC2 code provided by Bertschinger (2001) using the power spectrum given by BBKS. YNY calculated five runs, for a total number of 529 files, which were analyzed by the FoF (friends-of-friends) algorithm with a constant linking length of 0.2 times the mean particle separation.

I now discuss some limits and characteristics of N-body schemes. The N-body simulations used as comparisons neglect gaseous dissipation processes they are not SPH simulations. Thus the numerical mass function of YNY has the limits and reliability of the other numerical mass functions that neglect gaseous dissipation processes. Here I summarize the main limitations of this kind of N-body simulation.

There are two kinds of uncertainties in N-body simulations of collisionless systems. First, the dynamical equations are integrated numerically with less-than-perfect accuracy. Second, even exact solutions of these equations do not correspond to exact solutions of Collisionless Boltzmann and Poisson equations. Numerical errors are fairly easy to measure and control, but smoothing and discreteness effects have subtle implications for the interpretation of N-body simulations. Tests of N-body codes are hampered by a lack of exact solutions with which to compare the output of numerical integrations. Errors in numerical solutions include approximations introduced by the specific force calculation algorithm used, truncation caused by using a finite time-step, and roundoff due to finite computer wordlength. All can be treated as small perturbations introduced at each time-step; their cumulative effects can be estimated by monitoring the conservation of energy and momentum, or studied in more detail by running the same set of initial conditions with different time-steps and, in tree-codes, opening angles. Convergence testing shows that it is generally possible to constrain the uncertainty associated with numerical errors at a reasonable computational cost (e.g. Barnes & Hut 1989).

Another problem is relaxation. A standard technique to study the formation and evolution of gravitating systems is to perform an N-body simulation in which the mass distribution is discretised into a series of softened point particles. In this approach the particles represent a coarsegrained sampling of phase space which sets mass and spatial resolution. Unfortunately these super-massive particles will undergo two body encounters that lead to energy transfer as the system tends towards equipartition. In the real Universe the dark matter particles are essentially collisionless and pass each other unperturbed. The process of relaxation is difficult to quantify, but in the large N limit the discreteness effects inherent to the N-body technique vanish, so one uses as large a number of particles as computationally possible. Unfortunately in most cosmological simulations the importance of two body interactions does not vanish if one increases N. Structure formation in the cold dark matter (CDM) model occurs hierarchically since there is power on all scales, so the first objects that form in a simulation always contain only a few particles (Binney & Knebe 2002). With higher resolution the first structures form earlier and have higher physical densities because they condense out of a denser environment. Two body relaxation increases with density, so it

is not clear if increasing the resolution can diminish the overall amount of two body relaxation in a CDM simulation, i.e. if testing for convergence by increasing the mass resolution is appropriate (see Diemand 2004).

In order to have reliable results, it is necessary to properly furnish initial conditions. Advances in computational algorithms combined with the steady advance of computer technology have made it possible to simulate regions of the universe with unprecedented dynamic range (Bertschinger 1998).

The possibility to numerically resolve such vast dynamic ranges of length and mass raises the question of what the appropriate initial conditions are for such simulations. Hierarchical structure formation models like the cold dark matter (CDM) family of models have increasing amounts of power at smaller scales. This power should be present in the initial conditions. For simulations of spatially constant resolution, this is straightforward to achieve using existing community codes (Bertschinger 1995). However, investigators are increasingly using multiscale methods in which the best resolution is concentrated in only a small fraction of the simulation volume.

A satisfactory method to initialize multiscale simulations should satisfy several requirements in addition to correctly accounting for variable mass resolution. First, each refined field should preserve exactly the discretized long-wavelength amplitude and phase so as to truly refine the lower-resolution sample. Second, high-frequency power should be added in such a way that the multiscale fields are an exact sample of the power spectrum over the whole range of wavelengths sampled. Finally, a practical method should have a memory requirement and computational cost independent of refinement so that it is not limited by the size of the largest FFT that can be performed.

Bertschinger (2001) proposed a practical implementation of multiscale Gaussian random field sampling methods that meet these requirements (namely GRAFIC2). The essential idea enabling this development is that Gaussian random fields can be sampled in real space rather than Fourier space (hereafter k-space). Adaptive mesh refinement can then be performed conceptually in real space as is done in the nonlinear evolution code used by Abel et al. (2000).

In YNY, initial conditions are generated by the program developed and distributed by Bertschinger (2001) (GRAFIC2), while the fitting function for the power spectrum proposed by BBKS is adopted.

What is the dependence of the results on these initial choices and parameters? The multiplicity function depends on the initial condition as shown in Fig. 1 of the present paper and in Fig. 2 of YNY. As shown, changes in the parameters lead to not very large changes in the obtained multiplicity function. On the other hand, as shown by Jenkins et al. (2001), for a suitable halo definition, the simulated mass function is almost independent of epoch, cosmological parameters, and of initial power spectrum when expressed in appropriate variables.

4. Results

In this section, I compare the analytic multiplicity functions of PS, ST, J01, YNY7 and Eq. (18), of the present paper, with the numerical simulations of YNY. The numerical multiplicity functions are shown by crosses with errorbars in the five panels of Fig. 1 (Note that all figures have logarithmic abscissa). All the data from the initial redshift to the present $z = 0$ is compiled to draw the average curves (crosses) with error bars indicating the epoch to epoch variation. In the panel (f), all the numerical multiplicity functions are shown by thin lines.

Four analytic multiplicity functions described in the previous section are also shown in this figure, that is PS (solid line), ST (dotted line), J01 (long-dashed line), YNY7 (dashed line), and the one of the present paper described by Eq. (18) (dot-dashed line). Since the data are available only in the region at $\nu \leq 3$, these functions could be erroneous at $\nu \geq 3$.

Note that the comparison of the above curves with the results of N-body simulations show a very good agreement except for the PS model. However, there are some discrepancies between the YNY multiplicity function and other model functions (except the one in the present paper). First, the multiplicity function of the present paper, similarly to that of YNY, in the low-ν region of $\nu \leq 1$ systematically falls below the ST and the J01 functions. In this region the multiplicity function of the present paper is very close to that of YNY.

As seen in Fig. 1, and in agreement with YNY, the numerical multiplicity functions reside between the ST and J01 multiplicity functions at $2 \leq \nu \leq 3$ (except for the run 35b). Additionally, the numerical multiplicity functions have an apparent peak at $\nu \sim 1$ instead of the plateau that is seen in the J01 function.

On the other hand, in the high-ν region, where ν is significantly larger than unity, the multiplicity function of the present paper like YNY takes values between ST and J01 functions. These differences between numerical multiplicity functions and analytic ones, like ST, ST1 and J01, are within 1σ error bars, and they are possibly due to the different box sizes adopted (see YNY for a discussion). Throughout the peak range of $0.3 \leq \nu \leq 3$, the ST multiplicity function is in disagreement with the high mass resolution N-body simulations of YNY and that of the present paper. As shown by YNY the ST functional form provides a good fit to them only choosing parameter values of $a = 0.664$, $p = 0.321$, and $A_3 = 0.301$. The multiplicity function obtained in the present paper has a peak at $\nu \sim 1$ as in the ST function, and the YNY numerical multiplicity function and YNY7, instead of a plateau as in the J01 function.

The previous results are summarized in Fig. 2, where all the YNY N-body runs are plotted together. Note that Fig. 2 clearly shows that all the curves are compatible within the errors with the numerical simulation data there reported.

As shown in Figs. 1 and 2, the functional form proposed in YNY, namely YNY7, provides a better fit when compared with the ST functional form but it is not based on theory. The function obtained in this paper, similarly to YNY7, provides a better fit to simulations than the ST functional form, and at the same time has been obtained from solid physical, theoretical arguments. The better agreement observed between the multiplicity function of the present paper and YNY simulations, when compared with the ST, is connected to the shape of the barrier (δ_c). As reported in Sect. 2, taking account of the effects of asphericity and tidal interaction with neighbors,

Del Popolo & Gambera (1998) showed that the threshold is mass dependent, and in particular that in the set of objects that collapse at the same time, the less massive ones must initially have been denser than the more massive, since the less massive ones would have had to hold themselves together against stronger tidal forces.

The shape of the barrier given in Eq. (1) is a direct consequence of the angular momentum acquired by the protostructure during evolution while Eq. (2) introduces the effects of the cosmological constant.

Similarly to ST, the barrier increases with S (decrease with mass, M) differently from other models (see Monaco 1997a,b). The increase of the barrier with S has several important consequences and these models have a richer structure than the constant barrier model.

The decrease of the barrier with mass means that, in order to form structure, more massive peaks must cross a lower threshold, $\delta_c(\nu, z)$, than under-dense ones. At the same time, since the probability of finding high peaks is larger in more dense regions, this means that, statistically, in order to form structure, peaks in more dense regions may have a lower value of the threshold, $\delta_c(\nu, z)$, than those of under-dense regions. This is due to the fact that the resistance of an object to tides depends on its mass density, and for clumps having the same linear dimensions, on mass (less massive objects are more influenced by external tides), and consequently they must be more overdense to collapse by a given time. The angular momentum acquired by a shell centred on a peak in the CDM density distribution is anti-correlated with density: high-density peaks acquire less angular momentum than low-density peaks (Hoffman 1986; Ryden 1988). A larger amount of angular momentum acquired by low-density peaks (with respect to the high-density ones) implies that these peaks can more easily resist gravitational collapse and consequently it is more difficult for them to form structure. Therefore, on small scales, where the shear is statistically greater, structures need, on average, a higher density contrast to collapse.

The effect of a non-zero cosmological constant adds to that of L. The effect of a non-zero cosmological constant is that of slightly changing the evolution of the multiplicity function with respect to open models with the same value of Ω_0. This is caused by the fact that in a flat universe with $\Omega_\Lambda > 0$, the density of the universe remains close to the critical value later in time, promoting perturbation growth at lower redshift. The evolution is more rapid for larger values (in absolute value) of the spectral index, n.

As previously reported, the ST model gives a better fit to simulations than the PS model, but it has some discrepancies to the simulations. The ST model was introduced as a fit to the GIF simulations at the beginning (ST) and in a subsequent paper (SMT) the importance of aspherical collapse was recognized in the functional form of the mass function. The effects of asphericity were taken into account by changing the functional form of the critical overdensity (barrier) by means of a simple intuitive parameterization of elliptical collapse of isolated spheroids. The model proposed in the present paper is similar to ST and ST1 models, namely it uses the excursion set approach as extended by ST1 to calculate the multiplicity function, but at the same time it differs from ST and ST1 in the way the barrier was calculated and in the fact that takes account of angular momentum acquisition, and a non-zero cosmological constant, aspects not taken into account in ST and ST1. These differences gives rise to a multiplicity function in better agreement with simulations. This shows the importance of the form of the barrier.

The improvement of the multiplicity function of the present paper and ST with respect to PS is probably connected also to the fact that incorporating the non-spherical collapse with increasing barrier in the excursion set approach results in a model in which fragmentation and mergers may occur. These effects are important in structure formation.

In the case of non-spherical collapse with increasing barrier, a small fraction of the mass in the Universe remains unbound, while for the spherical dynamics, at a given time, all the mass is bound up in collapsed objects. Moreover, incorporating the non-spherical collapse with increasing barrier in the excursion set approach results in a model in which fragmentation and mergers may occur (ST). If the barrier decreases with S (Monaco 1997a,b), this implies that all walks are guaranteed to cross it and so there is no fragmentation associated with this barrier shape.

Thus the excursion set approach with a barrier taking account effects of the physics of structure formation gives rise to good approximations of the numerical multiplicity function: the approximation goodness increases with a more improved form of the barrier (taking account more physical effects: angular momentum acquisition, a non zero cosmological constant, etc.). Another important aspect of the quoted method is its noteworthy versatility: for example it is very easy to take account of the presence of a non-zero cosmological constant, englobing it in the barrier. The YNY numerical multiplicity function assumes a non-zero cosmological constant while the theoretical models (ST, ST1, J01) not take this into account.

Finally, I checked the time dependence of the multiplicity function. Figure 3 shows the multiplicity function from the 35a run, for four redshift ranges of $0 \leq z < 1$ (open circles), $1 \leq z < 3$ (open squares), $3 \leq z < 6$ (open triangles) and $z \geq 6$ (crosses). At high redshifts, high-ν halos in the exponential part of the YNY7 (solid line) function and Eq. 18) (dot-dashed line of the present paper) are probed. As redshift decreases, the probe window moves to the lower-ν region. Figure 3 shows that the multiplicity function of the present paper, Eq. (18), and YNY7 both give a good fit to the numerical simulations. For small values of ν, Eq. (18) is a slightly better fit to data, and at large values of ν the two functions decay in the same way.

The theoretical mass function of the present paper has also been compared with the numerical simulations of Reed et al. (2003) and Warren et al. (2005), and their fitting functions. Their results are compatible with that of YNY.

5. Conclusions

In the present paper, I compared the numerical multiplicity function given in YNY with the theoretical multiplicity function obtained with the excursion set model and an improved

version of the barrier shape obtained in Del Popolo & Gambera (1998), which implicitly takes account of tidal interactions between clusters and a non-zero cosmological constant. The barrier obtained in Del Popolo & Gambera (1998) gives rise to a better description of the multiplicity functions than other models (ST, J01) and the agreement is based on sound theoretical models and not on fit to simulations.

The main results of the paper can be summarized as follows:

1) The non-constant barrier of the present paper combined with the ST1 model gives "unconditional" multiplicity functions in better agreement with the N-body simulations of YNY than previous models (ST, ST1, J01).
2) The comparison of the theoretical multiplicity function of the present paper, in agreement with the YNY result, shows some discrepancies with the theoretical multiplicity function of several authors (ST, ST1, J01): e.g., the maximum value of the multiplicity function from simulations at $\nu \sim 1$ is smaller, and its low mass tail is shallower than the ST multiplicity function.
3) The multiplicity function of the present paper gives as good a fit to simulations results as the fit function proposed by YNY, but it was obtained from a sound theoretical background.
4) The excursion set model with a moving barrier is very versatile since it is very easy to introduce several physical effects in the calculation of the multiplicity function, by modifying the barrier.

The above considerations show that it is possible to obtain accurate predictions for a number of statistical quantities associated with the formation and clustering of dark matter haloes by incorporating non-spherical collapse which takes account of a non-zero cosmological constant in the excursion set approach. The improvement is probably also connected to the fact that incorporating non-spherical collapse with an increasing barrier in the excursion set approach results in a model in which fragmentation and mergers may occur, effects important in structure formation. Moreover, the effect of a non-zero cosmological constant adds to that of angular momentum, slightly changing the evolution of the multiplicity function with respect to open models with the same value of the matter density parameter.

References

Abel, T., Bryan, G. L., & Norman, M. L. 2000, ApJ, 540, 39
Bahcal, N. A., & Fan, X. 1998, ApJ, 504, 1
Bardeen, J. M., Bond, J. R., Kaiser, N., & Szalay, A. S. 1986, ApJ, 304, 15
Barnes, J. E., & Hut, P. 1989, ApJS, 70, 389
Bertschinger, E. 1995, COSMICS software release [arXiv:astro-ph/9506070]
Bertschinger, E. 1998, ARA&A, 36, 599
Bertschinger, E. 2001, APJS, 137, 1
Binney, J., & Knebe, A. 2002, MNRAS, 333, 378
Bond, J. R., Cole, S., Efsthatiou, G., & Kaiser, N. 1991, ApJ, 379, 440
Bower, R. G. 1991, MNRAS, 248, 332
Catelan, P., Lucchin, F., Matarrese, S., & Porciani, C. 1998, MNRAS, 297, 692
Davis, M., Efstathiou, G., Frenk, C. S., & White, S. D. M. 1985, ApJ, 292, 371
Del Popolo, A. 2002, MNRAS, 336, 8190
Del Popolo, A., & Gambera, M. 1998, A&A, 337, 96
Del Popolo, A., & Gambera, M. 1999, A&A, 344, 17
Del Popolo, A., & Gambera, M. 2000, A&A, 357, 809
Del Popolo, A., Ercan, E. N., & Xia, Z. Q. 2001, AJ, 122, 487
Diemand, J. 2004, Ph.D. Thesis
Efstathiou, G., Frenk, C. S., White, S. D. M., & Davis, M. 1988, MNRAS, 235, 715
Eisenstein, D. J., & Loeb, A. 1995, ApJ, 439, 520
Gelb, J. M., & Bertschinger, E. 1994, ApJ, 436, 467
Governato, F., Babul, A., Quinn, T., et al. 1999, MNRAS, 307, 949
Jenkins, A., Frenk, C. S., White, S. D. M., et al. 2001, MNRAS, 321, 372
Hoffman, Y. 1986, ApJ, 301, 65
Hoyle, F. 1949, in IAU and International Union of Theorethicaland Applied Mechanics Symposium, 195
Lacey, C., & Cole, S. 1993, MNRAS, 262, 627
Lacey, C., & Cole, S. 1994, MNRAS, 271, 676
Lin, L., Chiueh, T., & Lee, J. 2002, ApJ, 574, 527
Mo, H. J., & White, S. D. M. 1996, MNRAS, 282, 347
Monaco, P. 1997a, MNRAS, 287, 753
Monaco, P. 1997b, MNRAS, 290, 439
Nagashima, M., Totani, T., Gouda, N., & Yoshii, Y. 2001, ApJ, 557, 505
Peebles, P. J. E. 1969, ApJ, 155, 393
Press, W., & Schecter, P. 1974, ApJ, 187, 425
Reed, D., Gardner, Y., Quinn, T., et al. 2003, MNRAS, 346, 565
Ryden, B. S. 1988, ApJ, 329, 589
Sheth, R. K., & Lemson, G. 1999a, MNRAS, 304, 767
Sheth, R. K., & Lemson, G. 1999b, MNRAS, 305, 946
Sheth, R. K., & Tormen, G. 1999, MNRAS, 308, 119
Sheth, R. K., & Tormen, G. 2002, MNRAS, 329, 61 (ST)
Sheth, R. K., Mo, H. J., & Tormen, G. 2001, MNRAS, 323, 1 (SMT)
Sommer-Larse, J., & Dolgov, A. 2001, ApJ, 551, 608
Tozzi, P., & Governato, F. 1998, The Young Universe: Galaxy Formation and Evolution at Intermediate and High Redshift, ed. S. D'Odorico, A. Fontana, & E. Giallongo, ASP Conf. Ser., 146, 461
Warren, M. S., Abazajian, K., Holz, D. E., & Teodoro, L. 2005 [arXiv:astro-ph/0506395]
White, S. D. M. 1984, ApJ, 286, 38
White, M. 2002, ApJS, 143, 241
Yahagi, H. 2002, Ph.D. Thesis, University of Tokyo
Yahagi, H., & Yoshii, Y. 2001, ApJ, 558, 463
Yahagi, H., Nagashima, M., & Yoshii, Y. 2004, ApJ, 605, 709

Online Material

Appendix A

The effect of tidal torque on structure evolution has been studied in several papers especially in connection with the origin of galaxy rotation (Hoyle 1949; Peebles 1969; White 1984; Ryden 1988, hereafter R88; Eisenstein & Loeb 1995).

Following Eisenstein & Loeb (1995), we separate the universe into two distinct parts: the collapsing region, characterized by high density, and the rest of the universe. The boundary between these two regions is taken to be a sphere centered on the origin. As usual, in the following, we denote with $\rho(\boldsymbol{x})$ the density as function of space and $\delta(\boldsymbol{x}) = \frac{\rho(\boldsymbol{x})-\rho_{\rm b}}{\rho_{\rm b}}$. The gravitational force exerted on the spherical central region by the external universe can be calculated by expanding the potential, $\Phi(\boldsymbol{x})$, in spherical harmonics. Assuming that the sphere has radius R, we have:

$$\Phi(\boldsymbol{x}) = \sum_{l=0}^{\infty} \frac{4\pi}{2l+1} \sum_{m=-l}^{l} a_{\rm lm}(x) Y_{\rm lm}(\theta,\phi) x^l \tag{A.1}$$

where $Y_{\rm lm}$ are spherical harmonics and the tidal moments, $a_{\rm lm}$, are given by:

$$a_{\rm lm}(x) = \rho_{\rm b} \int_R^{\infty} Y_{\rm lm}(\theta,\phi)\rho(\boldsymbol{s}) s^{-l-1} {\rm d}^3 s. \tag{A.2}$$

In this approach the proto-structure is divided into a series of mass shells and the torque on each mass shell is computed separately. The density profile of each proto-structure is approximated by the superposition of a spherical profile, $\delta(r)$, and a random CDM distribution, $\varepsilon(\boldsymbol{r})$, which provides the quadrupole moment of the proto-structure. To the first order, the initial density can be represented by:

$$\rho(\boldsymbol{r}) = \rho_{\rm b}\left[1+\delta(r)\right]\left[1+\varepsilon(\boldsymbol{r})\right] \tag{A.3}$$

where $\varepsilon(\boldsymbol{r})$ is given by:

$$\left\langle |\varepsilon_k|^2 \right\rangle = P(k) \tag{A.4}$$

$P(k)$ being the power spectrum. The torque on a thin spherical shell of internal radius x is given by:

$$\tau(x) = -\frac{GM_{\rm sh}}{4\pi} \int \varepsilon(\boldsymbol{x}) \boldsymbol{x} \times \nabla\Phi(\boldsymbol{x}) {\rm d}\Omega \tag{A.5}$$

where $M_{\rm sh} = 4\pi\rho_{\rm b}\left[1+\delta(x)\right]x^2\delta x$. We are interested in the acquisition of angular momentum from the inner region, and for this purpose we take account only of the $l = 2$ (quadrupole) term. In fact, the $l = 0$ term produces no force, while the dipole ($l = 1$) cannot change the shape or induce any rotation of the inner region. As shown by Eisenstein & Loeb (1995), in the standard CDM scenario the dipole is generated at large scales, so the object we are studying and its neighborhood move as bulk flow with the consequence that the angular distribution of matter will be very small, then the dipole terms can be ignored. Because of the isotropy of the random field, $\varepsilon(\boldsymbol{x})$, Eq. (A.5) can be written as:

$$\left\langle |\tau|^2 \right\rangle = \sqrt(30)\frac{4\pi G}{5} A(x) \tag{A.6}$$

where

$$A(x) = \left[\left\langle a_{2m}(x)^2 \right\rangle \left\langle q_{2m}(x)^2 \right\rangle - \left\langle a_{2m}(x) q^*_{2m}(x) \right\rangle^2\right]^{1/2}$$

where $\langle\rangle$ indicates the mean value of the physical quantity considered. As stressed in the next section, following Eisenstein & Loeb (1995), the integration of the equations of motion ends at some time before the inner external tidal shell (i.e., the innermost shell of the part of the universe outside the sphere containing the ellipsoid) collapses. Then the inner region behaves as a density peak. This is important one in the development of the present paper.

What is the role of triaxiality of the ellipsoid (density peak) in generating a quadrupole moment? Equation (A.6) takes into account the quadrupole moment coming from the secondary perturbation near the peak. The density distribution around the inner region is characterized by a mean spherical distribution, δ, and a random isotropic field. In reality the central region is a triaxial ellipsoid. It is then important to evaluate the contribution to the quadrupole moment due to the triaxiality. Remembering that the quadrupole moments are given by:

$$\begin{aligned} q_{2\rm m} &= \int_{|\mathbf{r}|<R} Y^*_{2m}(\theta,\phi) s^2 \rho(\mathbf{s}) {\rm d}^3 s \\ &= \frac{x^2 M_{\rm sh}}{4\pi} \int Y^*_{2m}(\theta,\phi)\varepsilon(\boldsymbol{x}){\rm d}\Omega \end{aligned} \tag{A.7}$$

and approximating the density profile as:

$$\delta(\boldsymbol{x}) = \langle\delta(x)\rangle_{\rm Spherical} + \nu f(x) A(e,p) \tag{A.8}$$

$\langle\delta(x)\rangle_{\rm Spherical}$ being the mean spherical profile, $\nu = \frac{\delta}{\sigma}$ the peak height and σ the rms value of δ. The function $A(e,p)$ of the triaxiality parameters, e and p, is given by:

$$\begin{aligned} A(e,p) &= 3e\left(1-\sin^2\theta-\sin^2\theta\sin^2\phi\right) \\ &\quad + p\left(1-3\sin^2\theta\cos^2\phi\right) \end{aligned} \tag{A.9}$$

and the function $f(x)$ is given by (R88) by:

$$f(x) = \frac{5}{2\sigma} R_*^2 \left(\frac{1}{x}\frac{{\rm d}\xi}{{\rm d}x} - \frac{1}{3}\nabla^2\xi\right) \tag{A.10}$$

where ξ, σ and R_* are respectively the two-point correlation function, the mass variance and a parameter connected to the spectral moments (see Bardeen et al. 1986, Eq. (4.6d), hereafter BBKS). Substituting Eqs. (A.8) and (A.9) in Eq. (A.7) the sum of the mean quadrupole moments due to triaxiality is:

$$\frac{1}{M_{\rm sh}} \sum_{m=-2}^{2} \langle q_{2\rm m}(x)\rangle = \nu x^2 f(x) g(e,p) \tag{A.11}$$

where

$$g(e,p) = \left(\frac{1}{2\pi}\sqrt{6\pi/5}(e-p) + \frac{1}{4\pi}\sqrt{4\pi/5}(3e+p)\right)$$

which must be compared with that produced by the secondary perturbations, ε:

$$\left\langle q_{2\rm m}(x)^2 \right\rangle = \frac{x^4}{(2\pi)^3} M_{\rm sh}^2 \int k^2 P(k) j_2(kx)^2 {\rm d}k \tag{A.12}$$

where j_2 is the Bessel function of order 2. The values of e and p can be obtained from the distribution of ellipticity and prolateness (BBKS, Eq. (7.6) and Fig. 7) or for $\nu > 2$ by:

$$e = \frac{1}{\sqrt{5}x\left[1 + 6/\left(5x^2\right)\right]^{1/2}} \tag{A.13}$$

and

$$p = \frac{6}{5x^4\left[1 + 6/\left(5x^2\right)\right]^2} \tag{A.14}$$

(BBKS Eq. (7.7)). where x is given in BBKS (Eq. (6.13)). In the case of a peak with $\nu = 3$, we have $e \simeq 0.15$, $p \simeq 0.014$ while for peaks having $\nu = 2$ and $\nu = 1$ they are respectively given by $e \simeq 0.2$, $p \simeq 0.03$ and $e \simeq 0.25$ $p \simeq 0.04$.

For a 3σ profile, the source of quadrupole moment due to triaxiality is less important than that produced by the random perturbations ε in all the proto-structure, except in the central regions where the quadrupole moment due to triaxiality is comparable in magnitude to that due to secondary perturbations.

Thus, the triaxiality has a significant effect only in the very central regions, which contains no more than a few percent of the total mass and where the acquisition of angular momentum is negligible. It follows that the triaxiality can be ignored when computing both expansion and spin growth (R88). Moreover, as observed by Eisentein & Loeb (1995), the ellipsoid model does better in describing low shear regions (having higher values of ν), whose collapse is more spherical and then the effects of triaxiality are less evident. Only those peaks with at least $\nu > 2$, are studied in this paper. Even if the triaxiality was not negligible it contributes to increment the acquisition of angular momentum (Eisenstein & Loeb 1995), and has a greater effect on the density evolution (i.e., a larger reduction of the grow rate of the density).

In order to find the total angular momentum imparted to a mass shell by tidal torques, it is necessary to know the time dependence of the torque. This can be done connecting $q_{2\mathrm{m}}$ and $a_{2\mathrm{m}}$ to parameters of the spherical collapse model (Eisenstein & Loeb 1995, Eq. (A.13); R88, Eqs. (A.13) and (A.15)). Following R88 we have:

$$q_{2\mathrm{m}}(\theta) = \frac{1}{4} q_{2\mathrm{m},0} \overline{\delta}_0^{-3} \frac{(1-\cos\theta)^2 f_2(\theta)}{f_1(\theta) - \left(\frac{\delta_0}{\overline{\delta}_0}\right) f_2(\theta)} \tag{A.15}$$

and

$$a_{2\mathrm{m}}(\theta) = a_{2\mathrm{m},0}\left(\frac{4}{3}\right)^{4/3} \overline{\delta}_0 (\theta - \sin\theta)^{\frac{-4}{3}}. \tag{A.16}$$

The collapse parameter θ is given by:

$$t(\theta) = \frac{3}{4} t_0 \overline{\delta}_0^{-3/2} (\theta - \sin\theta). \tag{A.17}$$

Equations (A.15) and (A.16), by means of Eq. (A.6), give the tidal torque:

$$\tau(\theta) = \tau_0 \frac{1}{3}\left(\frac{4}{3}\right)^{(1/3)} \overline{\delta}_0^{-1} \frac{(1-\cos\theta)^2}{(\theta - \sin\theta)^{(4/3)}} \frac{f_2(\theta)}{f_1(\theta) - \left(\frac{\delta_0}{\overline{\delta}_0}\right) f_2(\theta)} \tag{A.18}$$

where $f_1(\theta)$ and $f_2(\theta)$ are given in R88 (Eq. (A.12)), τ_0 and $\delta_0 = \frac{\rho - \rho_\mathrm{b}}{\rho_\mathrm{b}}$ are respectively the torque and the mean fractional density excess inside the shell, as measured at the current epoch t_0. The angular momentum acquired during expansion can then be obtained integrating the torque over time:

$$L = \int \tau(\theta) \frac{\mathrm{d}t}{\mathrm{d}\theta} \mathrm{d}\theta. \tag{A.19}$$

The angular momentum obtained from Eq. (A.19) is evaluated at the time t_M. Then the calculation of the angular momentum can be solved by means of Eq. (A.19), once we have chosen the power spectrum. With the power spectrum and the parameters given in the next section and for a $\nu = 2$ peak, the model gives a value of 2.5×10^{74} g cm^2/s. We asssume that from t_M on, the ellipsoid has this constant angular momentum.

Appendix B

The equation governing the collapse of a density perturbation taking account of angular momentum acquisition by protostructures can be obtained using a model due to Peebles (Peebles 1993; see also Del Popolo & Gambera 1998, 1999).

Let us consider an ensemble of gravitationally growing mass concentrations and suppose that the material in each system collects within the same potential well with inward pointing acceleration given by $g(r)$ (see Del Popolo & Gambera 1998). We indicate with $\mathrm{d}P = f(L, rv_r, t)\mathrm{d}L\mathrm{d}v_r\mathrm{d}r$ the probability that a particle can be found in the proper radius range r, $r + \mathrm{d}r$, in the radial velocity range $v_r = \dot{r}$, $v_r + \mathrm{d}v_r$ and with angular momentum $L = rv_\theta$ in the range $\mathrm{d}L$. The radial acceleration of the particle is

$$\frac{\mathrm{d}v_r}{\mathrm{d}t} = \frac{L^2(r)}{M^2 r^3} - g(r) = \frac{L^2(r)}{M^2 r^3} - \frac{GM}{r^2}\cdot \tag{B.1}$$

Equation (B.1) can be derived from a potential and then from Liouville's theorem it follows that the distribution function, f, satisfies the collisionless Boltzmann equation:

$$\frac{\partial f}{\partial t} + v_r \frac{\partial f}{\partial r} + \frac{\partial f}{\partial v_r} \cdot \left[\frac{L_2}{r^3} - g(r)\right] = 0. \tag{B.2}$$

Assuming a non-zero cosmological constant Eq. (B.1) becomes:

$$\frac{\mathrm{d}v_r}{\mathrm{d}t} = -\frac{GM}{r^2} + \frac{L^2(r)}{M^2 r^3} + \frac{\Lambda}{3} r \tag{B.3}$$

(Peebles 1993; Bartlett & Silk 1993; Lahav 1991; Del Popolo & Gambera 1998, 1999). Integrating Eq. (B.3) we have:

$$\frac{1}{2}\left(\frac{\mathrm{d}r}{\mathrm{d}t}\right)^2 = \frac{GM}{r} + \int \frac{L^2}{M^2 r^3}\mathrm{d}r + \frac{\Lambda}{6} r^2 + \epsilon \tag{B.4}$$

where the value of the specific binding energy of the shell, ϵ, can be obtained using the condition for turn-around, $\frac{\mathrm{d}r}{\mathrm{d}t} = 0$.

In turn the binding energy of a growing mode solution is uniquely given by the linear overdensity, δ_i, at time t_i. From this overdensity, using linear theory, we can obtain that of the turn-around epoch and then that of the collapse. We find the binding energy of the shell, C, using the relation between v

and δ_i for the growing mode (Peebles 1980) in Eq. (B.4) and the linear overdensity at the time of collapse is given by:

$$\begin{aligned}\delta_{\rm c} &= \delta_{\rm co}\left[1+\int_{r_{\rm i}}^{r_{\rm ta}}\frac{r_{\rm ta}L^2\cdot {\rm d}r}{GM^3r^3}+\Lambda\frac{r_{\rm ta}r^2}{6GM}\right]\\ &\simeq \delta_{\rm co}\left[1+\frac{\beta_1}{\nu^{\alpha_1}}+\frac{\Omega_\Lambda\beta_2}{\nu^{\alpha_2}}\right]\end{aligned} \tag{B.5}$$

where $\alpha_1 = 0.585, \beta_1 = 0.46, \alpha_2 = 0.4$ and $\beta_2 = 0.02$.